Geothermics 88 (2020) 101899

Contents lists available at ScienceDirect

Geothermics

journal homepage: www.elsevier.com/locate/geothermics

Modelling water-rock interactions due to long-term cooled-brine reinjection in the Dogger carbonate aquifer (Paris basin) based on *in-situ* geothermal well data

Nicolas C.M. Marty*, Virginie Hamm, Christelle Castillo, Dominique Thiéry, Christophe Kervévan

BRGM, 3 Avenue Claude Guillemin, Orléans Cedex 2, 45064, France

ARTICLE INFO

Keywords:
Geothermal doublet
Porosity
Dogger
Aquifer
Water-Rock interaction
Geochemical modelling
Sonar

ABSTRACT

An experimental campaign was conducted using bottom-hole geometry data from a 24-year-old injection well (~1700 m deep) at a geothermal site exploiting the Dogger aquifer (Paris basin). A sonar tool was used to measure the geometry distortion of the open hole due to long-term reinjection of cooled brine. Reactive transport modelling was then performed. The calculated extent of carbonate dissolution at the well outlet was consistent with the sonar observations. The best fit to experimental results was obtained by considering partial CO_2 degassing in the reinjected brine, which is consistent with the artesian mode doublet operation.

1. Introduction

Located at a depth of 1500–2000 m, the carbonate Dogger reservoir is the main geothermal aquifer exploited in the Paris region of France. This geothermal resource heats approximately 210,000 dwellings in the Ile-de-France region (Hamm et al., 2016a) through a significant growth objective defined by the French energy transition law (http://www.gouvernement.fr/en/energy-transition). Energy exploitation involves the reinjection of cooled brine into the carbonate reservoir after calorie extraction by heat exchangers (*e.g.* Castillo et al., 2011a; Hamm et al., 2016a; Lopez et al., 2010). The local reinjected fluid temperature depends on the production temperature (55–85 °C), the energy requirements at the surface, and the operating flowrate (100–350 $m^3\ h^{-1}$) and typically varies between 40 and 60 °C with a minimum temperature of 35 °C. All the geothermal operations from the 1970s to 1990s operated according to this principle (Lopez et al., 2010); however, more recent geothermal operations conducted in the Dogger aquifer employ a heat pump (*e.g.* Arcueil-Gentilly, Bagneux, Neuilly-sur-Marne, etc.) to optimise the available geothermal resource, resulting in a lower return temperature. This implies that reinjection of cooled brines at the Dogger aquifer occurs at lower temperatures (approximately 25 °C) than previously (Cordier, 2013).

To date, the majority of studies on the thermal effect on the Dogger formation geochemistry have focused on the hydro-geochemical impact of the reinjection of hot fluids into the aquifer from the perspective of heat storage (Castillo et al., 2011b; Gille, 2010). Only a few studies have quantified the hydro-geochemical impact of cooled-fluid reinjection in a carbonate aquifer (Borozdina et al., 2012; Nick et al., 2015; Wong et al., 2016). Geothermal energy production in the carbonate Dogger formation began in the early 1970s in the Paris basin (Lopez et al., 2010). The typical lifetime of a geothermal doublet is approximately 30 years (duration of the initial operating permits); therefore, as older wells are shut down, new wells are commissioned. Thus, bottom-hole analysis of former injection wells could allow us to observe and quantify the effects of potential water-rock interactions induced by cooled-brine reinjection, especially in a carbonate aquifer such as the Dogger. Unfortunately, most of these wells were plugged when the abandonment procedure was completed and are thus inaccessible. However, as part of the CO_2-DISSOLVED project and through collaboration with the local geothermal operator (Chelles Chaleur, subsidiary of the Coriance group), the unique opportunity was granted to access the open-hole part of a former injection well in Chelles (Paris basin, France). This injector was utilised for 24 years from 1986 to 2010 but remains accessible as a backup injection well for the current geothermal doublet. An *in-situ* experimental campaign was conducted in March 2016 to analyse the reservoir geometry at the well outlet using a sonar tool provided and operated by Flodim (Cavity Survey and Well Logging Services Company, https://www.flodim.fr/).

The results of this study will aid our understanding of water-rock interactions at the well outlet, which is a major concern of the

* Corresponding author.
E-mail address: n.marty@brgm.fr (N.C.M. Marty).

https://doi.org/10.1016/j.geothermics.2020.101899
Received 7 November 2019; Received in revised form 27 May 2020; Accepted 28 May 2020

CO_2-DISSOLVED project (http://co2-dissolved.brgm.fr/). CO_2-DISSOLVED is an innovative carbon capture and storage (CCS) concept involving the capture, injection, and storage of dissolved CO_2 (rather than supercritical) in a deep saline aquifer coupled with geothermal heat recovery (Kervévan et al., 2013, 2014, 2017). Once out of the injection well, the acidified brine is expected to be chemically reactive with the reservoir porous matrix, particularly in the presence of carbonate minerals (Castillo et al., 2017; Gray et al., 2018; Snippe et al., 2020). In order to quantify these effects, both experimental and numerical modelling studies have been conducted in parallel as part of the CO_2-DISSOLVED project. The most notable results were obtained with the carbonate samples, showing the rapid development of a network of wormholes around the injection well outlet (Randi et al., 2014). A numerical simulation of this experiment performed with the MARTHE-PHREEQC code (Thiéry, 2015) reproduced reasonably well the massive dissolution of calcite near the injection well and the formation of wormholes due to the heterogeneous hydraulic conductivity (Randi et al., 2017). As demonstrated in numerous studies, the formation of wormholes depends on several parameters such as the ratios of reaction rate (*i.e.* Damköhler number), convection rate and diffusion rate (*i.e.* Peclet number) (*e.g.* Snippe et al., 2020; Randi et al., 2017; Izgec et al., 2010) and material heterogeneities (*i.e.* permeability and chemical composition) (*e.g.* Randi et al., 2017; Smith et al., 2013). Regarding the Chelles doublet, no dissolved CO_2 has been added in the injected cooled brine. Contrariwise, the artesian production mode of the doublet led to CO_2 degassing at surface. Near neutral pH of the reinjected brine resulted in a solution close to equilibrium with respect to calcite and therefore, the Damköhler number was low, thus promoting uniform dissolution (*e.g.* Snippe et al., 2020; Randi et al., 2017).

The aim of this study is to provide reference data for the predicted effects of reactive processes at the well outlet when reinjecting a cooled brine (*i.e.* a 'standard' cooled geothermal brine). Moreover, it is critical to be able to compare the modelling results to actual bottom-hole measured data in order to evaluate the validity of model predictions. In contrast to other geothermal reservoirs (*e.g.* Massiot et al., 2015, 2017), such reservoir data are extremely scarce for the Dogger carbonate aquifer and have not previously been made available to the scientific community; therefore, this study provides insights into water-rock interactions in this specific environment. The second objective of this study is to give insights to better interpret predictions of the CO_2-DISSOLVED system related to adding dissolved CO_2 to the reinjected brine. This is because this CCS method has not been tested yet at a full scale, so no equivalent *in-situ* data can be obtained; therefore, modelling remains the only approach to estimate the potential impacts of dissolved CO_2 reinjection on the exploited reservoir. In a such context, the hole stability (De Lary et al., 2015) and permeability increase leading to a risk of thermal breakthrough in the nearby production wells (Castillo et al., 2015, 2017) are intensively investigated.

2. Materials and methods

2.1. Chelles geothermal doublet

The Chelles geothermal district heating doublet was exploited continuously since its commissioning in 1986 until its closure in 2010 in artesian production mode with a maximal flow rate of 250 $m^3\ h^{-1}$ (Fig. 1). This system operated at high flow rates and wellhead pressures lower than the bubble point, leading to the partial release of gases initially dissolved in the Dogger pore water and their partial trapping in the geothermal pipe (Ungemach, 2001). The geothermal reservoir has a gas production capacity of approximately 0.125 m^3 per m^3 of Dogger fluid. The gas phase is mainly composed of CH_4 and other alkanes (55 %), N_2 (35 %), and CO_2 (10 %) (Ungemach, 2001; Marty et al., 1988; Criaud et al., 1987). From 2000 to 2010, a special degassing device was employed for gas extraction and burning (Ungemach, 2001). Unfortunately, gas extraction was not monitored over time; therefore, the partial pressure of CO_2 in equilibrium with the reinjected fluids remains uncertain. In contrast, flow and temperature data of the Chelles doublet GCHE1/GCHE2 are available from the Dogger database (http://sybase.brgm.fr/sybase/); however, data regarding the injection well are very sporadic between 1986 and 2010 (see injection_history file in Electronic Annex). Indeed, only typical injections have been recorded during winters of the first 5 years (one recording per year) and data are not continuous between years 5 to 24 (about one recording per month). Therefore, average flow rates and injection temperatures of the injection well (GCHE1) during summer (133 $m^3\ h^{-1}$ and 52 °C) and winter (148 $m^3\ h^{-1}$ and 48 °C) were considered in this study. Such a discretisation in two steps is supported by recorded data from similar doublets in the Paris basin (Lopez et al., 2010). Conversely, a constant temperature of 66 °C was monitored at the production well (GCHE2).

The section of the GCHE1 well has been drilled in 1985 with a diameter of 8½" (Figure S1 in supplementary material). However, the exact geometry of the open hole has not been determined after the drilling operation (*i.e.* no caliper measurement). Nonetheless, the numerous drilling operations carried out in the Dogger aquifer do not indicate any enlargement/damage of the borehole. In particular, for the GCHE4 well that has been drilled in 2013 at the immediate vicinity of GCHE1, using similar operational conditions in terms of tool (rotary drilling), geometry (8½" diameter), and geological formation targeted (Dogger aquifer), caliper data are available and they confirm an effective diameter of the open hole consistent with the nominal drilling diameter. As a consequence, we assumed an initial radius of 0.1 m for the open hole of the GCHE1 injection well. Regarding the structure of the geothermal reservoir, the GCHE1 well is characterised by five productive layers of the Dogger aquifer (Lopez et al., 2010; Hamm et al., 2016b): two layers of Comblachian units from −1668 m to −1683 m FOD (French Ordonance Datum), which contribute up to 14.7 % of the total flow, and three layers of Oolithic units from −1692 m to −1709 m FOD, contributing to 85.3 % of the total flow. The porosity, permeability, and flow contribution of each layer are summarised in Table 1. Measured permeabilities are greater than the one of the Oolithic limestone studied by Randi et al. (2017) (*i.e.* 88 mD). Such values may reflect the presence of fractures in the Dogger aquifer and raise the question about the upscaling of experiments carried out in laboratory.

2.2. Examination of the injection well in the post-geothermal production period

The injection well (GCHE1) integrity was examined in March 2016 (*i.e.* 6 years after its end of use) by combining ABI technique (Acoustic Borehole Imaging) and a sonar tool developed by Flodim. The technical principle of the sonar probe involves sound propagation (at lower frequency than for ABI) and recording the reflection of the acoustic signal against the cavity wall. The cavity wall is clearly imaged if the density contrast between the fluid and the ground is strong and the wall is regular. The measurement range is several centimetres to hundreds of metres. Currently, sonar does not allow continuous acquisition. The probe performs 360° rotations with a fixed measurement step (5° in this study) at a fixed depth. Once the rotation is complete, the probe moves to another depth to resume measurements.

2.3. Numerical tools

MARTHE-PHREEQC reactive transport modelling software is an extension of MARTHE software (http://marthe.brgm.fr/ – Thiéry, 2015), which has been upgraded by coupling with the PHREEQC chemical module (Parkhurst and Appelo, 2013). The coupling algorithm is purely sequential; at each time step, MARTHE computes the hydraulic head field and hence the velocity in the entire domain. It then transports all the considered dissolved chemical elements and transports heat to determine the temperature field on which geochemical

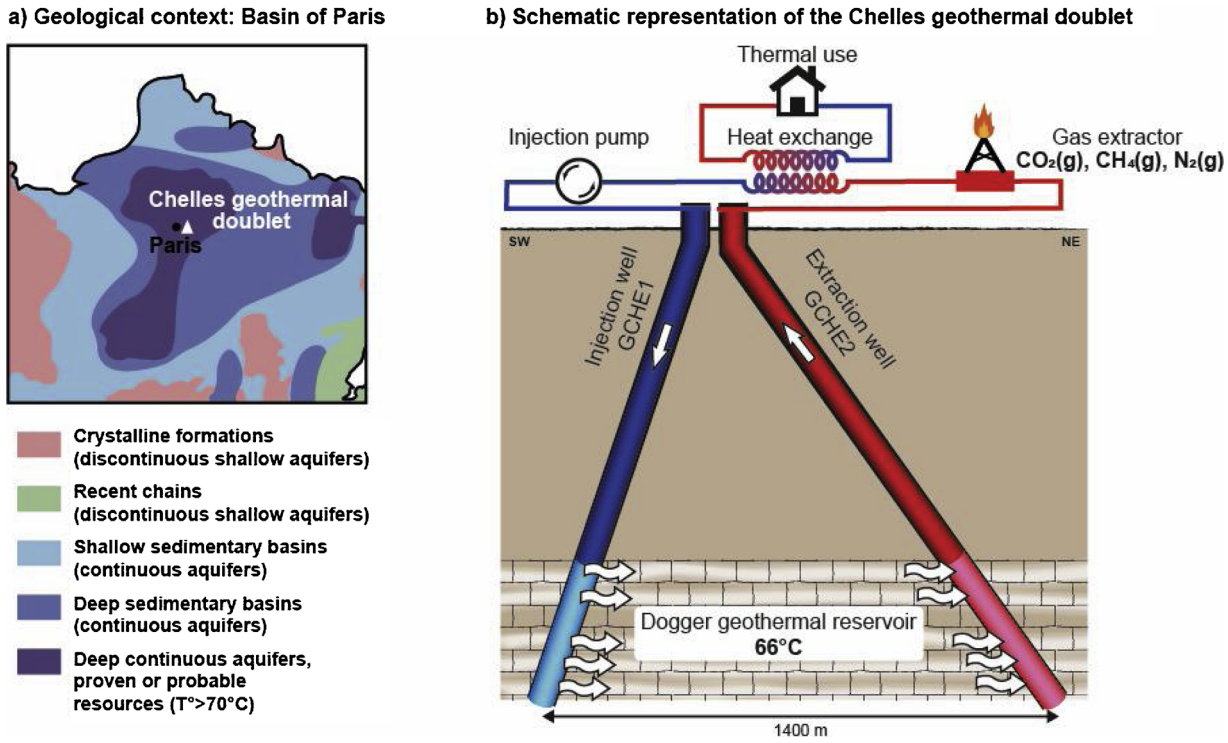

Fig. 1. Location (a) and schematic representation (b) of the Chelles geothermal doublet.

reactions depend. Then, the geochemistry is computed using the PHREEQC module. The THERMODDEM thermodynamic database (http://thermoddem.brgm.fr/ – Blanc et al., 2012) was used in this study. The database relies on the B-dot model, an extension of the Debye-Hückel activity model, valid up to salinities of about 1 mol L^{-1} (Hörbrand et al., 2018; Trémosa et al., 2014), which is consistent with the formation water salinity (see section 4.1).

3. Experimental results

The cavity extension was measured by the sonar tool with a depth step of ~0.5 m. Investigations were focused on the exploited part of the geothermal reservoir (from −1650 to −1710 m FOD), where the well is characterised by the absence of casing (open-hole). Maximum and minimum extensions are reported in Fig. 2. The shape and volume of the cavity were irregular in both horizontal and vertical orientations. Nonetheless, regardless of the amount of dissolved rock, preferential alteration leading to cavity formation was clearly identified in the SW direction. This observation fully agrees with the tilt of the GCHE1 well (Fig. 1); *i.e.*, the direction of injected flow strongly influences the shape of the formed cavity. Note that ABI data (GCHE1_ABI file in Electronic Annex) of the well section located below the productive layers do not indicate any enlargement/damage of the bore hole due to drilling operations, thus supporting the assumption of an initial open hole diameter of 0.1 m.

Surfaces and thus volumes of irregular polygons have been directly calculated by the tool software knowing the coordinates of the vertices and the thickness of the investigated area (Fig. 3a). Despite the observed slight shift of data with depth, the productive layers identified in 1985 (Table 1) were in reasonable agreement with the maximum altered volumes of rock. These volumes were converted to equivalent radii, assuming a cylindrical geometry for the cavity (Fig. 3b) following:

$$r_{eq} = \sqrt{\frac{V}{h \cdot \pi}} \quad (1)$$

where r_{eq} is the equivalent radius (m), V the volume given by the sonar tool (m^3) and h the thickness of the area investigated (m).

The average calculated radius was 0.21 m. Considering an initial well radius of 0.1 m, approximately 6 m^3 of the Dogger formation was dissolved during the operating period of the injection well (1986–2010). The average radius was compared with numerical results in order to evaluate the effect of various modelling assumptions (*i.e.* the geometry considered and the chemistry of the injection solution).

4. Modelling strategy

4.1. Dogger formation parameters

The mineralogical composition of the Dogger formation (Table 2) was established from the volume percentages given in André et al.

Table 1
Production levels identified by flowmetry analyses conducted in 1985.

Facies	Layer	Altitude (m FOD[a])	Flow contribution (%)	Porosity (%)	Permeability (D)
Comblachian	1	−1667.8 / −1669.8	7.3	12.5	1.03
	2	−1682.4 / −1683.3	7.4	15.8	2.09
Oolithic	3	−1692.1 / −1698.4	29.4	17.4	1.28
	4	−1702.3 / −1703.7	51.0	15.7	9.60
	5	−1707.1 / −1708.6	4.9	14.9	0.92

[a] French Ordnance Datum.

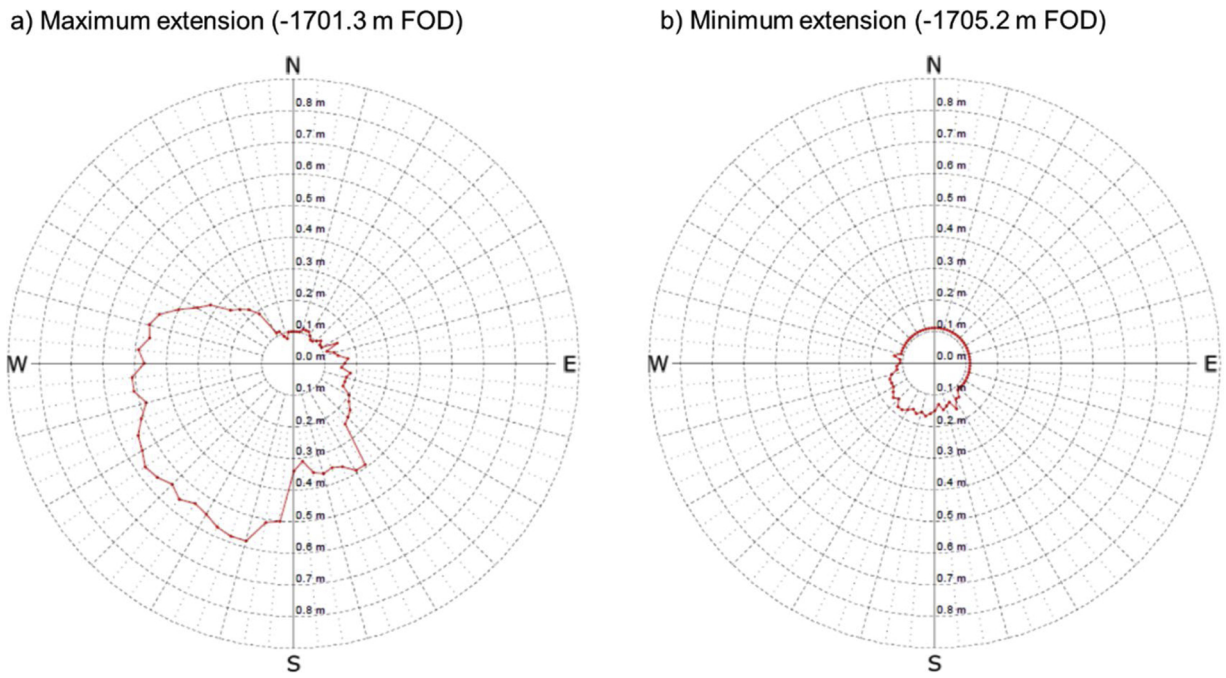

Fig. 2. a) Maximum extension of the cavity observed at -1701.3 m FOD and b) minimum extension of the cavity observed at -1705.2 m FOD. Experimental data were measured by the sonar tool every ~0.5 m.

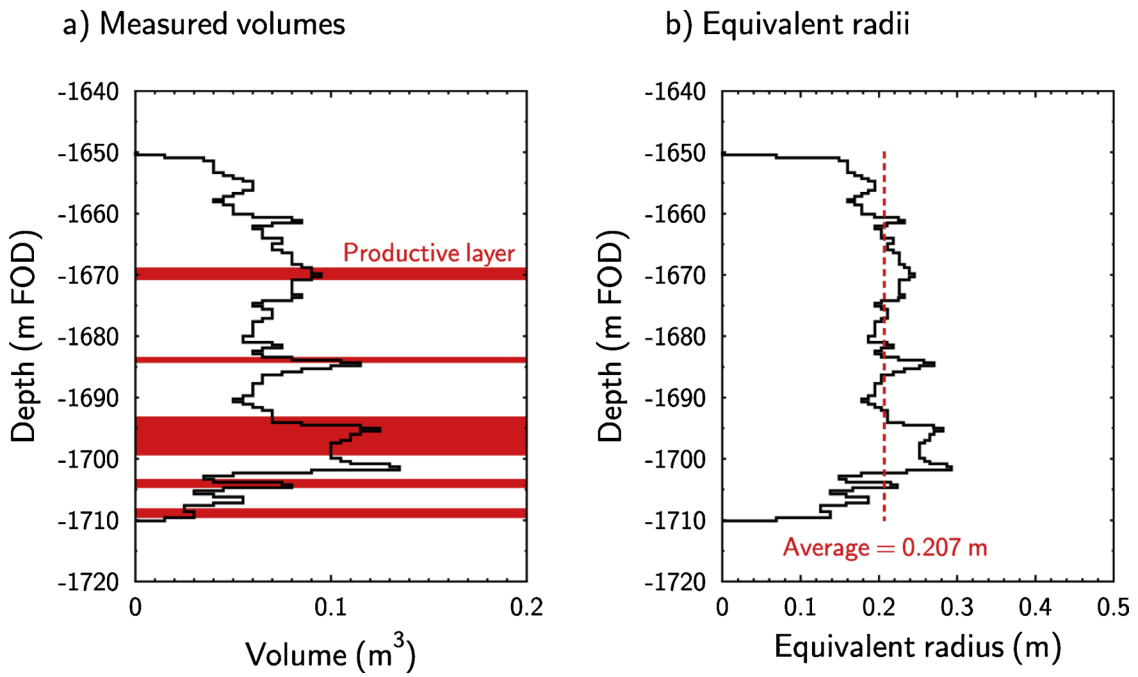

Fig. 3. a) Volumes measured by the sonar tool every 0.5 m and b) calculated equivalent radii assuming a cylindrical cavity.

Table 2
Mineralogical assemblage of the Dogger formation (data extracted from André et al. (2007) and Gille (2010)).

Mineral	Mineral name in THERMODDEM	Volume fraction
Calcite	Calcite	0.7
Dolomite-des	Dolomite(disordered)	0.1
Siderite	Siderite	0.05
Illite	Illite(IMt2)	0.05
Albite	Albite(low)	0.05
K-Feldspars	Microcline	0.05

(2007) and Gille (2010). The Dogger assemblage consists essentially of calcite and dolomite. Siderite, illite, albite, and K-feldspars are present as accessory minerals. The chemical composition of the Dogger brine was calculated for a temperature of 66 °C according to the value recorded at the production well. The simulation assumed a thermodynamic equilibrium between the Dogger pore water (Castillo et al., 2017; Criaud et al., 1989) and the mineralogical assemblage reported in Table 2. Note that the formation of albite and K-feldspars is unlikely at 66 °C and only dissolution reactions occurred during equilibration. In addition, a CO_2 partial pressure of 100 mbar (log pCO_2 = −1.0 atm) was assumed for the Dogger formation. Such a partial pressure is in the

Table 3
Chemistry of the Dogger pore water at 66 °C.

Element	Concentration (mol L^{-1})	Constraint
Al	$1.67\ 10^{-07}$	Gibbsite
Ba	$1.09\ 10^{-06}$	Barite
C(4)	$5.24\ 10^{-03}$	P_{CO2}
Ca	$1.12\ 10^{-02}$	Calcite
Cl	$3.14\ 10^{-01}$	
Fe	$8.39\ 10^{-05}$	Siderite
K	$9.38\ 10^{-03}$	Illite(IMt2)
Mg	$1.63\ 10^{-02}$	Dolomite-des
Na	$2.70\ 10^{-01}$	
S(6)	$9.01\ 10^{-03}$	
Si	$5.06\ 10^{-04}$	Quartz
Sr	$5.23\ 10^{-04}$	
pH	6.48	
pe	−3.51	
log P_{CO2} (atm)	−1.0	

Table 4
Saturation indices of the Dogger pore water at 66 °C (SI = log IAP/K, where IAP is the ionic activity product and K the thermodynamic constant).

Phases	Saturation indices (SI)
Calcite	0
Dolomite(disordered)	0
Siderite	0
Gibbsite	0
Illite(IMt2)	0
Albite(low)	0.48
Microcline	1.09
Quartz(alpha)	0
Celestite	−0.19
Barite	0

lower range of values reported for this aquifer (Coudrain-Ribstein et al., 1998). Constraints assumed for the fluid composition calculation are reported in Table 3. The fluid is in equilibrium with carbonates (calcite, dolomite, and siderite), illite, and quartz (Table 4). It is also close to equilibrium with sulphate bearing minerals such as barite ($BaSO_4$) and celestite ($SrSO_4$).

4.2. Chemistry of injected fluids

The numerical simulations considered fluid reinjection at different temperatures according to different periods (heat extraction being more important in cold periods). In the heat exchanger, calculations did not consider the mineralogical assemblage of the Dogger because no mineral phase was theoretically present. However, potential secondary phases such as calcite, and barite were implemented. If oversaturated, their precipitation should occur primarily in the heat exchanger and in the downstream pipe portion (*i.e.* in the coldest zone).

As a first approximation, CO_2 degassing was not considered and the fluid chemistry at 48 °C and 52 °C was calculated from simple cooling of the Dogger pore water ("No degassing" case, Table 5). As expected, the temperature decrease destabilises the carbonate minerals, which are then undersaturated (Table 6). However, between 1986 and 2010, the Chelles geothermal doublet operated in artesian mode, resulting in degassing at the wellhead that favoured carbonate precipitation. A second model ("Partial degassing" case, Table 5) was then established assuming partial degassing of CO_2 until a calcite saturation index of −0.01 was reached (*i.e.* almost in equilibrium with this carbonate). This value was adjusted to reasonably match with the observed calcite dissolution using a single-layer geometry. Finally, a third solution chemistry was calculated considering the CO_2 atmospheric partial pressure (*i.e.* log P_{CO2} = −3.45 atm) related to calcite precipitation ("Total degassing" case, Table 5). Regardless of the fluid chemistry (*i.e.* CO_2 degassing), the cooling of brines leads to barite and quartz precipitation (Table 6). Nonetheless, silica precipitation is known to be a slow process at considered temperatures (Rimstidt and Barnes, 1980) and Si concentrations reported in Table 5 are probably underestimated. Note that numerous studies have reported quartz, barite, and calcite scaling in geothermal wells (Bozau et al., 2015, Tarcan et al., 2008, Akin et al., 2015); however, this study was not focused on such surface and subsurface processes.

4.3. Geometries and key modelling assumptions

Two distinct but simplified geometries were considered: homogeneous and heterogeneous (Fig. 4). A single-layer homogeneous model was first applied to simulate the geothermal reservoir. The mesh was of radial type with X, Y, and Z coordinates coinciding with the radius, angle, and layer of the model, respectively. A homogeneous porosity of 15 % was assumed in the geological formation (*i.e.* average porosity – Lopez et al., 2010). The model assumed upper and lower impervious walls following the approximate analytical solution of Vinsome and Westerveld (1980) (thermal conduction perpendicular to the aquifer) implemented in MARTHE. This analytical solution avoids the vertical discretisation of the clay layers, so it considerably reduces the number of grid cells in the model, thereby decreasing the computation time. Note that a single-layer geometry without the consideration of impervious walls leads to an overestimation of the cooling down of the reservoir (Le Brun et al., 2011). Moreover, even if several productive layers have been identified (Table 1), the open hole extension shown on Fig. 3b appears to be relatively homogeneous and thus a single layer geometry could be a correct assumption for assessing mineralogical transformations. A second, heterogeneous model was proposed using the Chelles injection well data (*e.g.* the productive layers identified by flowmeter, Table 1). The Dogger reservoir was discretised into five layers with specific properties. The mesh was also of radial type and we assumed upper and lower impervious walls, using an analytic solution for the heat diffusion. Injected flows were distributed according to the contribution of the productive layers (Table 1). In contrast, according to flowmeter data, unproductive layers were considered as impervious layers only contributing to heat diffusion. The general parameters used for the simulations were defined using data from previous literature and are summarised in Table 7. A radial extension of 1000 m was assumed whatever the geometry considered.

5. Numerical results and discussion

The numerical results for the single-layer model are predominantly focused on the mineralogical evolution whereas those for the multi-layer model mainly deal with porosity modifications and temperature profiles. According to the work of Castillo et al. (2017), gibbsite, gibbsite, quartz, goethite, barite, anhydrite, hydromagnesite, and celestite were selected here as potential secondary minerals. Note that the hydromagnesite phase was considered instead of magnesite (another Mg-carbonate) because the latter forms at temperatures above 60–80 °C (Gautier et al., 2014). Similarly, precipitation of anhydrite rather than gypsum was assumed because the predicted temperatures were over 40 °C (Hill, 1937).

5.1. Single-layer geometry

Calcite alteration was observed in the near field of the injection well (from 0 to <1.5 m, Fig. 5). The numerical results were affected by the modelling assumptions; calcite alteration decreased from "No degassing" to "Partial degassing", and then to "Total degassing" cases. Regardless of the injected fluids (Table 5), the model indicated dolomite dissolution up to about 15 m from the injection well occurring concomitantly with calcite precipitation (from >1.5 to 15 m, Fig. 5).

Table 5
Injected brine compositions as a function of temperature and CO_2 partial pressure.

Element	Concentrations (mol L^{-1})					
	No degassing		Partial degassing		Total degassing	
	48 °C	52 °C	48 °C	52 °C	48 °C	52 °C
Al	$4.15\ 10^{-08}$	$5.67\ 10^{-08}$	$6.02\ 10^{-08}$	$7.59\ 10^{-08}$	$1.67\ 10^{-07}$	$1.67\ 10^{-07}$
Ba	$7.12\ 10^{-07}$	$7.89\ 10^{-07}$	$7.12\ 10^{-07}$	$7.90\ 10^{-07}$	$6.94\ 10^{-07}$	$7.68\ 10^{-07}$
C(4)	$5.24\ 10^{-03}$	$5.24\ 10^{-03}$	$4.71\ 10^{-03}$	$4.80\ 10^{-03}$	$4.01\ 10^{-04}$	$3.70\ 10^{-04}$
Ca	$1.12\ 10^{-02}$	$1.12\ 10^{-02}$	$1.12\ 10^{-02}$	$1.12\ 10^{-02}$	$9.64\ 10^{-03}$	$9.63\ 10^{-03}$
Cl	$3.14\ 10^{-01}$	$3.14\ 10^{-01}$	$3.14\ 10^{-01}$	$3.14\ 10^{-01}$	$3.14\ 10^{-01}$	$3.14\ 10^{-01}$
Fe	$8.39\ 10^{-05}$	$8.39\ 10^{-04}$	$8.39\ 10^{-05}$	$8.39\ 10^{-05}$	$1.61\ 10^{-06}$	$1.25\ 10^{-06}$
K	$9.38\ 10^{-03}$	$9.38\ 10^{-03}$	$9.38\ 10^{-03}$	$9.38\ 10^{-03}$	$9.38\ 10^{-03}$	$9.38\ 10^{-03}$
Mg	$1.63\ 10^{-02}$	$1.63\ 10^{-02}$	$1.63\ 10^{-02}$	$1.63\ 10^{-02}$	$1.63\ 10^{-02}$	$1.63\ 10^{-02}$
Na	$2.70\ 10^{-01}$	$2.70\ 10^{-01}$	$2.70\ 10^{-01}$	$2.70\ 10^{-01}$	$2.70\ 10^{-01}$	$2.70\ 10^{-01}$
S(6)	$9.01\ 10^{-03}$	$9.01\ 10^{-03}$	$9.01\ 10^{-03}$	$9.01\ 10^{-03}$	$9.01\ 10^{-03}$	$9.01\ 10^{-03}$
Si	$3.30\ 10^{-04}$	$3.64\ 10^{-04}$	$3.30\ 10^{-04}$	$3.65\ 10^{-04}$	$3.40\ 10^{-04}$	$3.76\ 10^{-04}$
Sr	$5.23\ 10^{-04}$	$5.23\ 10^{-04}$	$5.23\ 10^{-04}$	$5.23\ 10^{-04}$	$5.23\ 10^{-04}$	$5.23\ 10^{-04}$
pH	6.50	6.49	6.70	6.64	7.78	7.77
pe	−3.24	−3.31	−3.50	−3.49	−4.77	−4.82
log P_{CO2} (atm)	−1.14	−1.11	−1.34	−1.26	−3.45	−3.45

Table 6
Saturation indices of injected brines as a function of temperature and CO_2 degassing (SI = log IAP/K, where IAP is the ionic activity product and K the thermodynamic constant).

Mineral name in THERMODDEM	Saturation indices (SI)					
	No degassing		Partial degassing		Total degassing	
	48 °C	52 °C	48 °C	52 °C	48 °C	52 °C
Calcite	−0.20	−0.16	−0.01	−0.01	0	0
Dolomite (disordered)	−0.59	−0.46	−0.21	−0.16	−0.12	−0.08
Siderite	−0.21	−0.17	−0.03	−0.03	−1.69	−1.79
Illite (IMt2)	−0.77	−0.59	−0.38	−0.30	−0.07	−0.23
Albite (low)	0.11	0.19	0.30	0.34	0.81	0.74
Microcline	0.96	0.99	1.16	1.14	1.66	1.54
Quartz (alpha)	0	0	0	0	0	0
Celestite	−0.24	−0.23	−0.24	−0.23	−0.23	−0.21
Barite	0	0	0	0	0	0
Goethite	−0.59	−0.48	−0.25	−0.22	0	0

Dolomite/ankerite conversion (approximately equivalent to dolomite/calcite conversion) has been observed in several experiments (Debure et al., 2017; Gysi and Stefánsson, 2012); thus, even if such reaction progress is probably overestimated (*i.e.* minerals processed at local equilibrium), a similar process is expected to occur in the Dogger formation. Note that the amount of precipitated calcite was also promoted by the Ca concentrations in the injected fluids (Table 5) and the amount of mineral is lower for the "Total degassing" case. Regarding other mineralogical transformations, the amounts of microcline and albite remained constant. Considering the low amounts of accessory minerals (illite and siderite) as well as precipitated secondary minerals (gibbsite, quartz, goethite, and barite), their impact on porosity evolution were very limited; these numerical results are reported in the Supplementary Data. The formation of anhydrite, hydromagnesite, and celestite was not observed in any simulation case.

Table 7
General parameters used for the simulations.

Simulation parameters	Values
Initial temperature (°C)	66
Volumetric heat capacity of the mineral (J m^{-3} $°C^{-1}$)	2.10^6
Heat capacity of the water (J kg^{-1} $°C^{-1}$)	4185
Thermal conductivities of the mineral (W m^{-1} $°C^{-1}$)	2.5
Thermal conductivities of the water (W m^{-1} $°C^{-1}$)	0.6
Molecular diffusion (m^2 s^{-1})	$1.5\ 10^{-10}$
Mesh refinement (m)	0.025-20
Time step (month)	1
Division of the time step	33000

As calcite and dolomite constitute 80 % of the initial mineralogical assemblage of the Dogger formation (Table 2), modelling assumptions

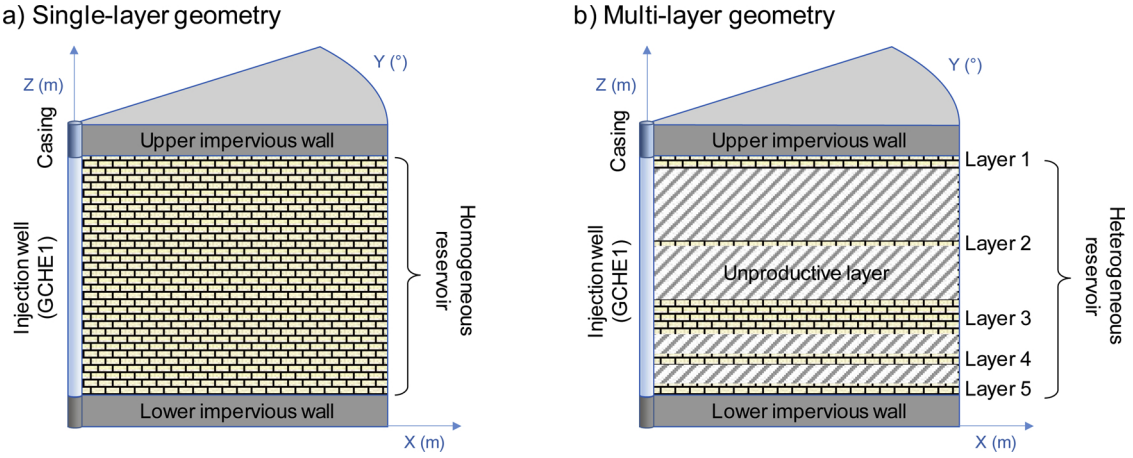

Fig. 4. Schematic representations of the two model geometries: a) single-layer geometry and b) multi-layer geometry based on flowmeter data (1985).

Table 8
Open-hole extension modelled for the multi-layer geometry. No degassing, partial degassing and total degassing correspond to modelling assumptions made on fluid chemistries (see section 4.2).

Productive layer	Observed radius (m)		Modelled radius (m)		
	min-max	average	No degassing	Partial degassing	Total degassing
1	0.23 – 0.25	0.24 ± 0.01	2.03	0.37	0.1[a]
2	0.21 – 0.28	0.24 ± 0.02	2.96	0.56	0.1[a]
3	0.21 – 0.29	0.25 ± 0.02	2.23	0.45	0.1[a]
4	0.14 – 0.25	0.19 ± 0.05	6.16	1.18	0.1[a]
5	0.11 – 0.14	0.13 ± 0.01	1.89	0.38	0.1[a]

[a] no extension, 0.1 m being the initial radius of the borehole.

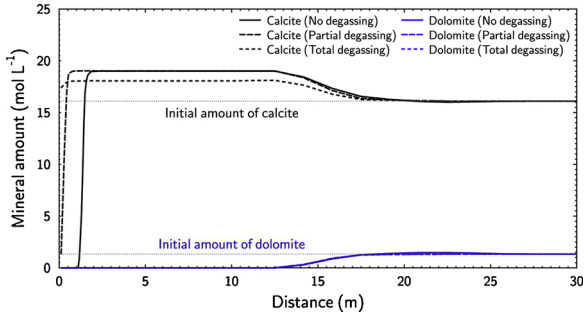

Fig. 5. Calcite ($CaCO_3$) and dolomite ($CaMg(CO_3)_2$) profiles calculated with the single-layer model after 24 years of cooled brine injection. No degassing, partial degassing, and total degassing correspond to the different modelling cases based on injected fluid chemistry (see section 4.2).

affected the resulting porosity (Fig. 6a) while temperature profiles remained identical whatever the injected fluid chemistry (Fig. 6b). The experimental results indicated an average radius of 0.21 m for the open hole. The modelling case omitting gas extraction ("No degassing" model) showed total dissolution of carbonate minerals up to 1 m around the injection well; the enlargement of the open hole around the injection well was clearly overestimated. In contrast, the numerical modelling indicated that total degassing of the cooled injected fluid was unlikely as its effect on porosity was very limited (*i.e.* no significant variation around the injection well). Additionally, the low Ca concentration of the injected fluid (Table 5) limited the calcite precipitation promoted by the dolomite/calcite conversion and a slight porosity increase was predicted despite the molar volumes of minerals (*i.e.* 36.9 $cm^3\ mol^{-1}$ for calcite and 32.2 $cm^3\ mol^{-1}$ for dolomite, as expressed per mole of CO_3^{2-}). Finally, only partial CO_2 degassing of the injected fluid could explain the field observations. According to the work of Deng et al. (2017), dissolution of 35 % is a reasonable threshold for a fast-reacting mineral (*i.e.* calcite), above which erosion of the altered layer occurs. Following the removal of the altered layer, the open-hole aperture increases. Assuming an initial porosity of 15 % in the current model, a porosity increase of more than 50 % would lead to disaggregation of the remaining matrix. The remaining minerals (*e.g.* albite and microcline) are expected to fall to the bottom of the injection well or be further transported. The "Partial degassing" model led to a porosity increase of up to 50 % at 0.25 m (Fig. 6a). An open-hole aperture of 0.25 m was then estimated, which is in reasonable agreement with the experimental data. Note that more recent doublets use both immerged and surface pumps, at the production and injection wells, respectively, to keep fluids under pressure and prevent the brine

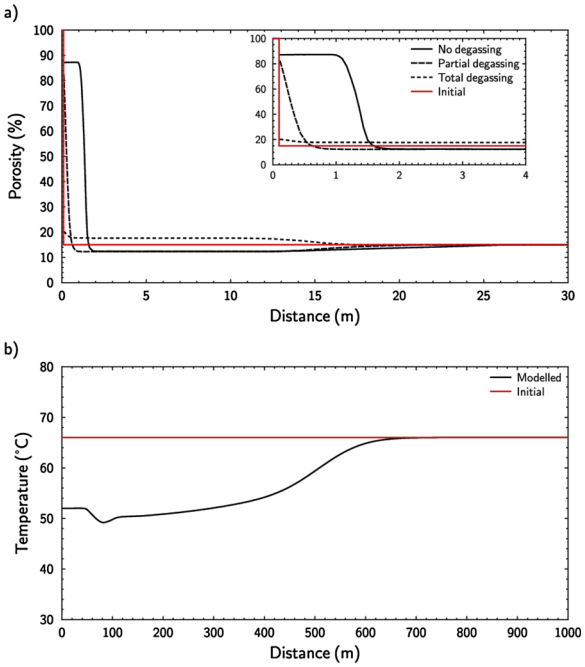

Fig. 6. a) Porosity profiles calculated with the single-layer model after 24 years of cooled brine injection. No degassing, partial degassing, and total degassing correspond to the different modelling cases based on injected fluid chemistry (see section 4.2). b) Temperature profile calculated with the single-layer model after 24 years of cooled brine; results are identical for all the injected fluid chemistries considered.

from reaching the bubble point (Lenoir, 1992). Therefore, the porosity profile obtained without degassing corresponds to the open-hole diameter increase that could be expected in recent doublets.

5.2. Multi-layer geometry

Mineralogical transformations calculated using the multi-layer model were similar to those already described with the single-layer model; the open-hole enlargement is caused by carbonate dissolution. Therefore, only the porosity profiles after 24 years of geothermal production are reported in Fig. 7 whereas open-hole extensions are given in Table 8. As already observed with the previous model, the absence of fluid degassing led to an overestimation of open-hole formation (up to 6.2 m for layer 4). In contrast, the porosity change that was modelled assuming that total degassing was negligible. The best fit to the experimental data was obtained considering partial degassing of injected fluids. Assuming a threshold of 35 % for carbonate alteration (Deng et al., 2017) and specific initial porosities for each layer (Table 1), the numerical results indicated a final open-hole radius ranging from 0.37 m (layer 1) to 1.18 m (layer 4). Nonetheless, the reactivity of unproductive layers may buffer the alteration of productive layers, which is therefore likely to be overestimated if those unproductive layers are assumed to be impermeable. Such a reactivity is confirmed by experimental results effectively showing an alteration of layers identified as unproductive from flowmeter measurements (Fig. 3). This explains why the use of a single-layer geometry allowed a better approximation of the alteration front progression in the Dogger aquifer.

The geothermal doublet system induces the formation of a "cold bubble" in the reservoir around the injector (Hamm et al., 2016a; Castillo et al., 2011a). The migration of the "cold bubble" was similar regardless of fluid chemistry assumptions and therefore, only one temperature profile is reported on Fig. 8. After 24 years of geothermal production, the cold injection front progressed up to 700 m, which corresponds to half the distance between the injection and the production wells at depth. The numerical results indicated that a decrease

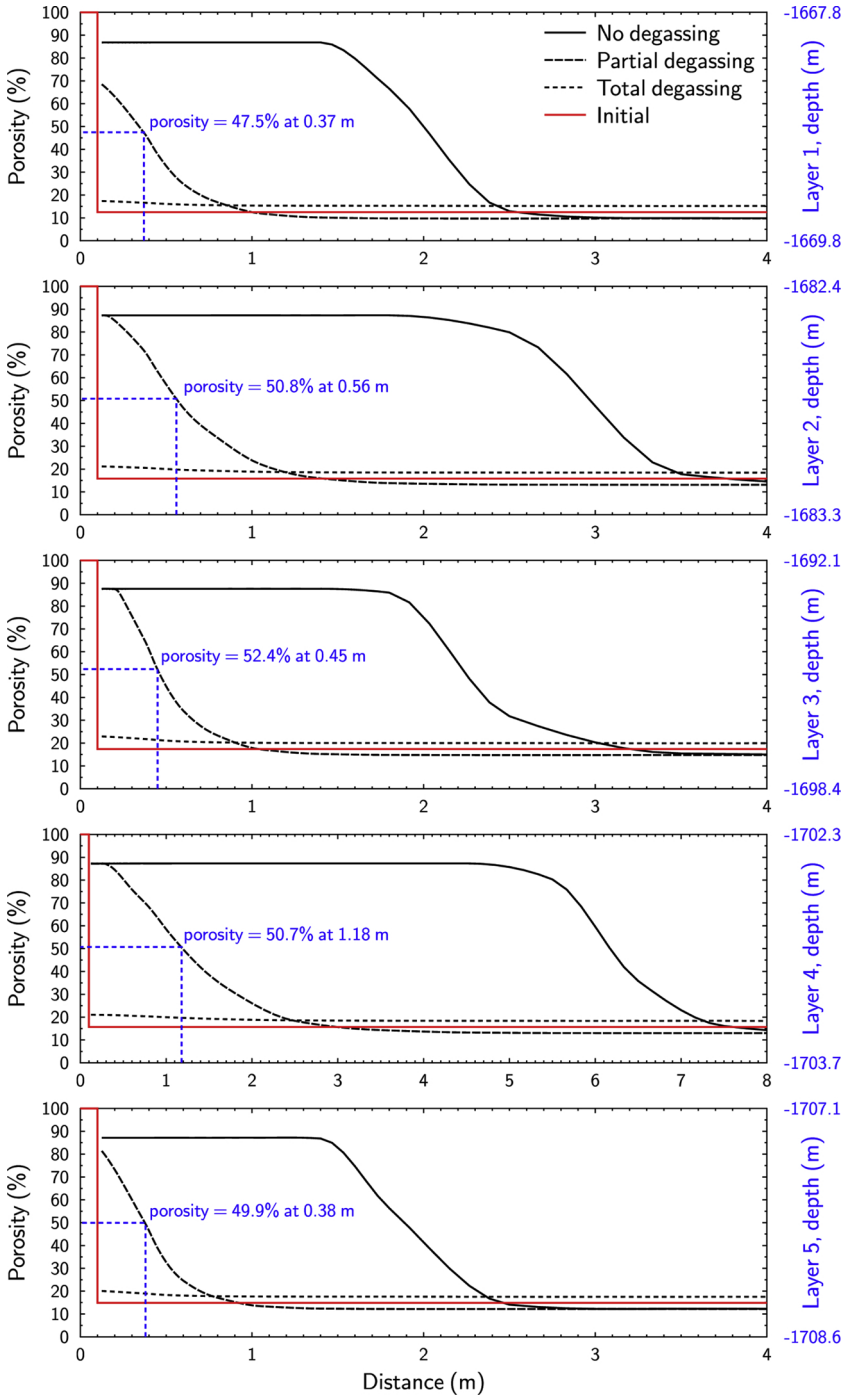

Fig. 7. Porosity profiles calculated with the multi-layer model after 24 years of cooled brine injection. No degassing, partial degassing and total degassing correspond to modelling assumptions made on fluid chemistries (see section 4.2).

in temperature at the production well was unlikely and was in accordance with recorded data (*i.e.* no thermal breakthrough). Nonetheless, numerous studies have shown a dissymmetry of the temperature profile resulting from the shape of the velocity profile induced by fluid extraction at the production well (*e.g.* Castillo et al., 2017); the production well has been neglected here as the modelling of the exact progression of the "cold bubble" was not an objective of this study. The consideration of two injection periods (48 °C in winter and 52 °C in summer) led to an inhomogeneous temperature profile in the near field of the injection well. Consistent with the temperature dependence of the mineral solubility (Blanc et al., 2012), both the temperature decrease and the mass transport led to a calcite alteration that was attenuated when enabling CO_2 degassing.

5.3. Model limitations

The modelling results of open-hole extension remain uncertain because several processes can affect its progression. The effects of porosity changes on the resulting permeability were neglected in this study. Following the Kozeny-Carman equation, a porosity increase would lead to a permeability increase favouring mass transport and rock alteration. In contrast, the particles released by cement alteration could be mobilised and transported further, where particle re-deposition could cause clogging in the productive layer and a reduction of permeability (Deng

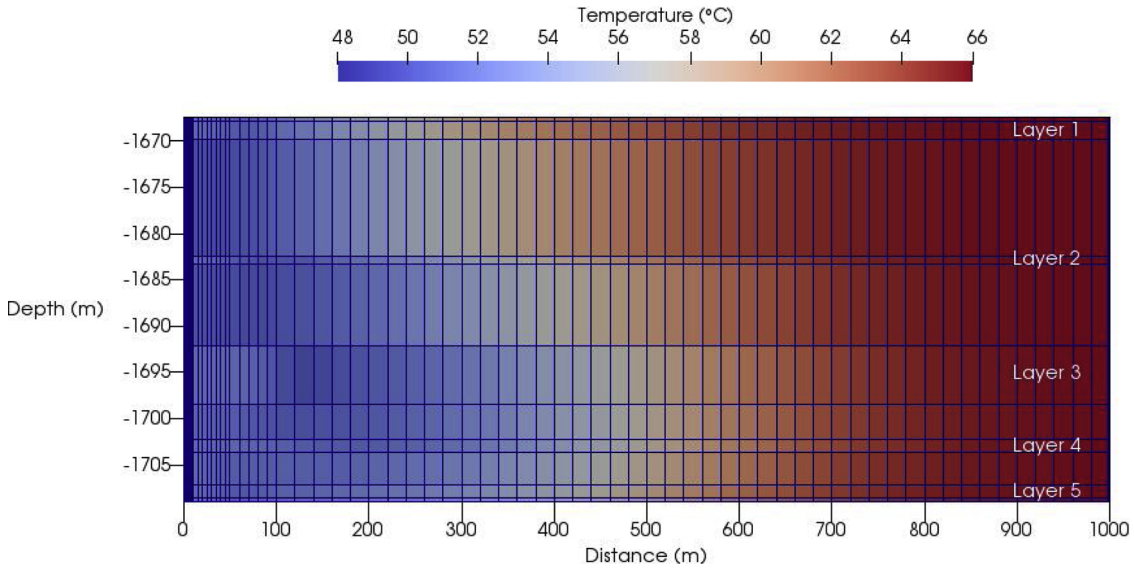

Fig. 8. Temperature profile calculated with the multi-layer model after 24 years of cooled brine injection. Note that results were identical whatever modelling assumptions made on fluid chemistries (see section 4.2).

et al., 2017; Sbai and Azaroual, 2011). Unfortunately, the balance between higher porosity leading to higher permeability and porosity clogging by particles leading to a decrease of mass transport properties is difficult to determine. Therefore, our models assumed constant permeability and imposed average flow rates monitored at GCHE1. Moreover, the reinjection of cooled brine in the GCHE1 borehole could have a thermomechanical impact on the integrity of the reservoir rock that cannot be considered by MARTHE-PHREEQC. The current sonar technique is limited to the identification of open-hole walls and cannot detect porosity increases inside the rock matrix and/or the possible formation of wormholes in carbonate rocks (Randi et al., 2017; Ott and Oedai, 2015). However, despite these uncertainties, the model and field results were in reasonable agreement, even if a simplified geometry was considered. Nevertheless, the non-iterative sequential coupling algorithm of the MARTHE-PHREEQC code implies using a relatively small time step fulfilling the Neumann criterion, thus leading to a high number of iterations and then a high computation time (*i.e.* several days). The time step used for this study (80 s, Table 7) is the best compromise we have found between calculation efficiency and numerical dispersion possibly observed when the Neumann criterion is not strictly respected, which is the case for the smallest cells at the immediate vicinity of the well. However, keeping in mind that for all these cells, water-rock interactions rapidly became negligible as calcite was entirely dissolved, time step could be relaxed without negative consequence on calculation accuracy.

6. Conclusions

Field investigations of the Chelles former injection well after 24 years of continuous geothermal operation offered a novel opportunity to evaluate reservoir mineralogical transformations at the well outlet induced by cooled-brine reinjection during a typical geothermal exploitation period. Sonar data acquired on the open-hole part of this well showed significant and uneven distortion of the initial cylindrical geometry. The investigation technique, used for the first time in the Paris basin, is a promising tool for borehole examinations, especially when a camera is not usable due to groundwater turbidity as in the Dogger aquifer.

Using parameters as close as possible to actual well operation data as well as simplified geometries that are widely used in predictive modelling, this study attempted to quantify the water-rock interaction processes in the near-well area of the exploited reservoir. Because of the partial monitoring of production data and more specifically a lack of data on the chemistry of the injected fluids (*e.g.* rate of CO_2 degassing) as well as drawbacks of current reactive transport software (*e.g.* transport of eroded particles is not accounted for), the accuracy of the numerical results had some limitations. Nonetheless, the simulation results confirmed significant carbonate alterations in the near-well part of the reservoir on the same orders of magnitude as the average measured open-hole aperture (0.21 m). This gave us more confidence in our modelling approach and suggested that the observed geometry alteration could mainly have a geochemical origin. Best-fit results were obtained for partial CO_2 degassing in the reinjected brine, which is also consistent as the geothermal doublet was operated in artesian mode.

Although previous studies on the CO_2-DISSOLVED concept involving cooled CO_2-rich brine reinjection in a geothermal well (*i.e.* CO_2 concentration less than 1 mol L^{-1} under field conditions, so that CO_2 remains entirely dissolved in brine) used a similar modelling approach, they lacked reference field data for evaluating the predictive capability of the models. Therefore, the results of this study, based on unique bottom-hole data showing the geochemical impact of brine reinjection in a “standard” geothermal doublet, constitute a valuable baseline for future calibration of reactive transport models. These reactive transport models could then be more confidently used to perform the pre-dimensioning calculations of dissolved CO_2 injection in a doublet, which forms the first operational test-phase of the CO_2-DISSOLVED system.

Declaration of Competing Interest

The authors declare that they have no known competing financial interests or personal relationships that could have appeared to influence the work reported in this paper.

Acknowledgments

The authors thank the anonymous reviewers for their comments and

suggestions. This work was supported by the ANR (French National Research Agency), within the framework of the "CO_2-DISSOLVED" project (ANR-12-SEED-0009), and Geodenergies (http://www.geodenergies.com/), as part of the "PILOTE CO_2-DISSOLVED" project. A part of this work was also supported by ADEME (French agency of ecological transition) in the framework of the research project INJECT-DOGGER (2016-2017) which evaluated the impact on the reservoir porosity and permeability for different reinjection temperature. The authors would also like to thank Chelles Chaleur and Coriance for making the well available to our team during the three-day experimentation period. FLODIM are also greatly acknowledged for applying their proprietary sonar investigation tool to the novel context of a former geothermal injection well. The authors thank O. Audouin from CFG (Compagnie Française de Géothermie, https://www.cfgservices.fr/en/) for his technical support on the well characterisation.

Appendix A. Supplementary data

Supplementary material related to this article can be found, in the online version, at doi:https://doi.org/10.1016/j.geothermics.2020.101899.

References

André, L., Audigane, P., Azaroual, M., Menjoz, A., 2007. Numerical modeling of fluid–rock chemical interactions at the supercritical CO2–liquid interface during CO2 injection into a carbonate reservoir, the Dogger aquifer (Paris Basin, France). Energy Convers. Manage. 48, 1782–1797.

Akin, T., Guney, A., Kargi, H., 2015. Modeling of calcite scaling and estimation of gas breakout depth in a geothermal Well by using PHREEQC. Proceedings of the 40th Workshop on Geothermal Reservoir Engineering.

Blanc, P., Lassin, A., Piantone, P., Azaroual, M., Jacquemet, N., Fabbri, A., Gaucher, E.C., 2012. Thermoddem: a geochemical database focused on low temperature water/rock interactions and waste materials. Appl. Geochem. 27, 2107–2116.

Borozdina, O., Ratouis, T., Ungemach, P., Antics, M., 2012. Thermochemical modelling of cooled brine injection into low enthalpy sedimentary reservoirs. Geothermal Res. Council Trans. 36, 151–157.

Bozau, E., Häußler, S., van Berk, W., 2015. Hydrogeochemical modelling of corrosion effects and barite scaling in deep geothermal wells of the North German Basin using PHREEQC and PHAST. Geothermics 53, 540–547.

Cordier, E., 2013. Modélisation Numérique d'un Doublet Géothermique Exploitant Le Dogger Dans Le Secteur De Bagneux Dans Le Cadre De l'étude De Faisabilité d'un Doublet Géothermal Mise En Œuvre Par Le SIPPEREC. Synthèse Des Calculs, in.

Castillo, C., Azaroual, M., Ignatiadis, I., Goyeneche, O., 2011a. Geochemical Parameters As Precursors to Predict the Decline of Temperature in the Dogger Aquifer (Paris Basin, France). Thirty-Sixth Workshop on Geothermal Reservoir Engineering, Stanford (California), United States, pp. 8p.

Castillo, C., Azaroual, M., Hamm, V., Jacquemet, N., 2011b. Physico-chimie Et Réactivité Des Fluides Du Dogger Du Bassin Parisien Soumis Aux Conditions De Stockage De Chaleur, in, BRGM/RP-60189-FR.

Criaud, A., Fouillac, C., Marty, B., Brach, M., Wei, H.F., 1987. Gas Geochemistry of the Dogger Geothermal Aquifer (Paris Basin, France). Twelfth Workshop on Geothermal Reservoir Engineering, Stanford (California), United States.

Castillo, C., Kervévan, C., Thiéry, D., 2015. Geochemical and reactive transport modeling of the injection of cooled Triassic brines into the Dogger aquifer (Paris basin, France). Geothermics 53, 446–463.

Castillo, C., Marty, N.C.M., Hamm, V., Kervévan, C., Thiéry, D., de Lary, L., Manceau, J.-C., 2017. Reactive transport modelling of dissolved CO2 injection in a geothermal doublet. Application to the CO2-DISSOLVED concept. Energy Procedia 114, 4062–4074.

Criaud, J., Giot, D., Le Nindre, Y., Criaud, A., Fouillac, C., Brach, M., Menjoz, A., Martin, J.-C., Lambert, M., 1989. Caractérisation et modélisation du réservoir géothermique du Dogger, Bassin Parisien, France., in, Rapport final BRGM-GTH. IRG SGN 89, 240.

Coudrain-Ribstein, A., Gouze, P., de Marsily, G., 1998. Temperature-carbon dioxide partial pressure trends in confined aquifers. Chem. Geol. 145, 73–89.

De Lary, L., Manceau, J.-C., Loschetter, A., Rohmer, J., Bouc, O., Gravaud, I., Chiaberge, C., Willaume, P., Yalamas, T., 2015. Quantitative risk assessment in the early stages of a CO_2 geological storage project: implementation of a practical approach in an uncertain context. Greenh. Gases Sci. Technol. 5, 50–63.

Deng, H., Voltolini, M., Molins, S., Steefel, C., DePaolo, D., Ajo-Franklin, J., Yang, L., 2017. Alteration and Erosion of rock matrix bordering a carbonate-rich shale fracture. Environ. Sci. Technol. 51, 8861–8868.

Debure, M., Andreazza, P., Canizarès, A., Grangeon, S., Lerouge, C., Mack, P., Madé, B., Simon, P., Veron, E., Warmont, F., Vayer, M., 2017. Study of iron-bearing dolomite dissolution at various temperatures: evidence for the formation of secondary nanocrystalline iron-rich phases on the dolomite surface. ACS Earth Space Chem. 1, 442–454.

Gille, A.L., 2010. Suivi Et Modélisation Du Comportement Hydro-géochimique Du Dogger, Soumis à La Réinjection De Fluides « Chaud » Et « Froid » Université Pierre et Marie Curie, École nationale supérieure des Mines de Paris, Centre d'informatique Géologique de Fontainebleau.

Gysi, A.P., Stefánsson, A., 2012. CO2-water–basalt interaction. Low temperature experiments and implications for CO2 sequestration into basalts. Geochim. Cosmochim. Acta 81, 129–152.

Gray, F., Anabaraonye, B., Shah, S., Boek, E., Crawshaw, J., 2018. Chemical mechanisms of dissolution of calcite by HCl in porous media: simulations and experiment. Adv. Water Resour. 121, 369–387.

Gautier, Q., Bénézeth, P., Mavromatis, V., Schott, J., 2014. Hydromagnesite solubility product and growth kinetics in aqueous solution from 25 to 75 °C. Geochim. Cosmochim. Acta 138, 1–20.

Hill, A.E., 1937. The transition temperature of gypsum to anhydrite. J. Am. Chem. Soc. 59, 2242–2244.

Hamm, V., Bouzit, M., Lopez, S., 2016a. Assessment of complex well architecture performance for geothermal exploitation of the Paris basin: a modeling and economic analysis. Geothermics 64, 300–313.

Hamm, V., Treil, J., Receveur, M., 2016b. Gestion Du Dogger Et Corrélation Entre Niveaux Producteurs, in, BRGM/RP-65472-FR.

Hörbrand, T., Baumann, T., Moog, H.C., 2018. Validation of hydrogeochemical databases for problems in deep geothermal energy. Geotherm. Energy 6, 20.

Izgec, O., Zhu, D., Hill, A.D., 2010. Numerical and experimental investigation of acid wormholing during acidization of vuggy carbonate rocks. J. Pet. Sci. Eng. 74, 51–66.

Kervévan, C., Bugarel, F., Galiègue, X., Le Gallo, Y., May, F., O'Neil, K., Sterpenich, J., 2013. CO2-Dissolved: A Novel Approach to Combining CCS and Geothermal Heat Recovery, in: EAGE (Ed.) Sustainable Earth Sciences (SES). technologies for sustainable use of the deep sub-surface, Pau, France.

Kervévan, C., Beddelem, M.H., O'Neil, K., 2014. CO_2-DISSOLVED: a novel concept coupling geological storage of dissolved CO_2 and geothermal heat recovery – part 1: assessment of the integration of an innovative low-cost, water- based CO_2 capture technology. Energy Procedia 63, 4508–4518.

Kervévan, C., Beddelem, M.H., Galiègue, X., Le Gallo, Y., May, F., O'Neil, K., Sterpenich, J., 2017. Main results of the CO2-DISSOLVED project: first step toward a future industrial pilot combining geological storage of dissolved CO2 and geothermal heat recovery. Energy Procedia 114, 4086–4098.

Lenoir, D., 1992. Geothermal exploitation of the Dogger in the Paris basin maintenance, renewal and reliability of the geothermal loop. Geothermics 21, 855–860.

Le Brun, M., Hamm, V., Lopez, S., Ungemach, P., Antics, M., Yves Ausseur, J., Cordier, E., Giuglaris, E., Goblet, P., Lalos, P., 2011. Hydraulic and thermal impact modelling at the scale of the geothermal heating doublet in the Paris Basin, France. In: 36th Stanford Geothermal Workshop. Stanford, United States. pp. 403–416.

Lopez, S., Hamm, V., Le Brun, M., Schaper, L., Boissier, F., Cotiche, C., Giuglaris, E., 2010. 40 years of Dogger aquifer management in Ile-de-France, Paris Basin, France. Geothermics 39, 339–356.

Marty, B., Criaud, A., Fouillac, C., 1988. Low enthalpy geothermal fluids from the Paris sedimentary basin—1. Characteristics and origin of gases. Geothermics 17, 619–633.

Massiot, C., McNamara, D.D., Nicol, A., Townend, J., 2015. Fracture width and spacing distributions from borehole televiewer logs and cores in the rotokawa geothermal Field, New Zealand. In: World Geothermal Congress 2015. International Geothermal Association.

Massiot, C., Townend, J., Nicol, A., McNamara, D.D., 2017. Statistical methods of fracture characterization using acoustic borehole televiewer log interpretation. J. Geophys. Res. Solid Earth 122, 6836–6852.

Nick, H.M., Wolf, K.-H., Brhun, D., 2015. Mixed CO2-Water injection into geothermal reservoirs: a numerical study. In: Proceedings World Geothermal Congress 2015. Melbourne, Australia.

Ott, H., Oedai, S., 2015. Wormhole formation and compact dissolution in single- and two-phase CO2-brine injections. Geophys. Res. Lett. 42, 2270–2276.

Parkhurst, D.L., Appelo, C.A.J., 2013. Description of Input and Examples for PHREEQC Version 3 - a Computer Program for Speciation, Batch-reaction, One-dimensional Transport, and Inverse Geochemical Calculations, in, U.S. Geological Survey Techniques and Methods,, Book 6, Chap. A43, 497. available only at. http://pubs.usgs.gov/tm/06/a43.

Rimstidt, J.D., Barnes, H.L., 1980. The kinetics of silica-water reactions. Geochim. Cosmochim. Acta 44, 1683–1699.

Randi, A., Sterpenich, J., Morlot, C., Pironon, J., Kervévan, C., Beddelem, M.H., Fléhoc, C., 2014. CO2-DISSOLVED: a novel concept coupling geological storage of dissolved CO_2 and geothermal heat recovery – part 3: design of the MIRAGES-2 experimental device dedicated to the study of the geochemical water-rock interactions triggered by CO_2 laden brine injection. Energy Procedia 63, 4536–4547.

Randi, A., Sterpenich, J., Thiéry, D., Kervévan, C., Pironon, J., Morlot, C., 2017. Experimental and numerical simulation of the injection of a CO2 saturated solution in a carbonate reservoir: application to the CO2-DISSOLVED concept combining CO2 geological storage and geothermal heat recovery. Energy Procedia 114, 2942–2956.

Sbai, M.A., Azaroual, M., 2011. Numerical modeling of formation damage by two-phase particulate transport processes during CO2 injection in deep heterogeneous porous media. Adv. Water Resour. 34, 62–82.

Smith, M.M., Sholokhova, Y., Hao, Y., Carroll, S.A., 2013. CO2-induced dissolution of low

permeability carbonates. Part I: characterization and experiments. Adv. Water Resour. 62, 370–387.
Snippe, J., Berg, S., Ganga, K., Brussee, N., Gdanski, R., 2020. Experimental and numerical investigation of wormholing during CO2 storage and water alternating gas injection. Int. J. Greenh. Gas Control. 94, 102901.
Tarcan, G., Gemici, Ü., Aksoy, N., 2008. Hydrogeochemical factors effecting the scaling problem in Balçova geothermal field, İzmir, Turkey. Environ. Geol. 58, 1375.
Thiéry, D., 2015. Modélisation 3D Du Transport Réactif Avec Le Code De Calcul MARTHE v7.5 Couplé Aux Modules Géochimiques De PHREEQC, in: R. BRGM/RP-65010-FR (Ed.). available at. Orléans, France, pp. 164. http://infoterre.brgm.fr/rapports/RP-65010-FR.pdf.
Trémosa, J., Castillo, C., Vong, C.Q., Kervévan, C., Lassin, A., Audigane, P., 2014. Long-term assessment of geochemical reactivity of CO2 storage in highly saline aquifers: application to Ketzin, in Salah and Snøhvit storage sites. Int. J. Greenh. Gas Control. 20, 2–26.
Ungemach, P., 2001. Mise En Service Opérationnelle d'une Ligne De Dégazage: Brûlage Du Biogaz Géothermal Sur Le Doublet De Chelles, in: L'énergie Du Sous-sol. La Géothermie En Ile-de-france. Bulletin N°2. http://www.geothermie-perspectives.fr/sites/default/files/bulletin-gth-idf-02.pdf.
Vinsome, P., Westerveld, J., 1980. A simple method for predicting cap and base rock heat losses in thermal reservoir simulators. J. Can. Pet. Technol. 19 0-2276.
Wong, C., Buscarlet, E., Addison, S., Brun, M., 2016. Reactive Transport Modelling of Injection Fluid-Reservoir Rock Interaction. New Zealand Geothermal Workshop, Auckland, New Zealand.